J. S. Afr. Inst. Min. Metall., vol. 88, no. 1.
Jan. 1988. pp. 27-39.

Excess shear stress in the assessment of geologically hazardous situations*

by J.A. RYDER†

SYNOPSIS

A high proportion of damaging rockbursts are thought to be underlain by seismic events that represent shear or rupture along planes of weakness (faults, joints, dyke contacts). Such events are controlled by shear stresses and friction properties along the plane. Excess shear stress (ESS) is a measure that can be evaluated numerically and that, in principle, can be used in an assessment of the possible magnitude and relative likelihood of seismic activity.

Methods for the calculation of ESS in practical mining contexts, and for the estimation of the magnitudes of possible seismic event progressions, are briefly reviewed. The effects of variables such as depth, stoping width and, in particular, virgin horizontal stresses on general shear-type seismic hazards are investigated. Attempted back-analyses of two large rockbursts are described.

SAMEVATTING

Daar word gereken dat seismiese gebeurtenisse wat afskuiwing of breuke langs swak vlakke (verskuiwings, nate, gesteentegangkontakte) verteenwoordig, ten grondslag lê van 'n hoë persentasie beskadigende rotsbarstings. Sulke gebeurtenisse word beheer deur skuifspannings en wrywingseienskappe langs die vlak. Oormatige skuifspanning (OSS) is a maatstaf wat numeries geëvalueer kan word, en in beginsel, gebruik kan word vir die bepaling van die moontlike grootte en relatiewe waarskynlikheid van seismiese aktiwiteit.

Daar word 'n kort oorsig gegee van metodes vir die berekening van die OSS in praktiese mynbouverband en die raming van die grootte van reekse seismiese gebeurtenisse. Die uitwerking van veranderlikes soos diepte, afboudikte en veral horisontale oerspannings op algemene skuiftipe seismiese gevare word ondersoek. Pogings om terugontledings van twee groot rotsbarstings te doen, word beskryf.

Introduction

Rockbursts and other manifestations of high rock stress are the scourge of deep-level mining, especially in the vicinity of certain geological structures such as dykes and faults, which have long been known[1,2] to enhance rockburst activity. This has been confirmed by numerous mine seismic networks, which show that seismic events tend to locate or cluster near particular 'hazardous' structures[3-6].

A widely used measure of severity of mining conditions, introduced by Cook[2] in the 1960s, is the concept of energy release rate (ERR). ERR has been found to correlate well with depth of face fracturing[7], hangingwall conditions[4], and the decreases in seismicity observed after the introduction of stabilizing pillars in a number of deep mines[8]; it is the preferred criterion used in current designs of stabilizing pillar and backfill systems[9]. ERR can be evaluated analytically or, in more general situations, by the use of numerical stress analysis programs such as MINSIM-D[10]. It is actually a mathematical property associated with the faces of tabular excavations set in *homogeneous elastic* ground. As such, ERR has little to say about the hazard-amplifying effects of geological structures *per se*: what are needed here are more concrete physical pictures, as well as more specifically structured hazard criteria, than are furnished by the more global ERR index taken in isolation.

The present paper discusses one such model, which is thought to have particular relevance for geological structures that take the form of pre-existing planes of weakness. It is not essentially novel: the basic model is a simplification and expression in mining terms of a standard seismological representation of earthquake events, and shear-stress criteria in various forms are routinely used by geotechnical engineers in assessing the stability of jointed structures in general.

In addition, it must be stressed that this excess shear stress (ESS) model has by no means yet acquired the status of ERR in terms of field verifications of applicability, nor are the calibrations of certain key parameters currently well understood. Nevertheless, ESS analyses have potential in due course to make a useful contribution to the design of safer mining layouts in geologically disturbed areas and in deep-level mining in general.

Classes of Seismic Events

Based on first-motion evidence, mining seismologists have proposed[5,6,11,12] that mine seismicity falls into at least two classes: one associated with the crushing of highly stressed volumes of rock (which gives 'anomalous' seismic signatures), and the other with slip or rupture along planes in the rockmass (which gives normal earthquake-type seismic signatures). To throw some light on the possible nature of these classes, Fig. 1 shows the state of stress around the advancing face of a typical isolated tabular excavation at depth.

In front of the immediate face is a zone, C, which is

* Presented at the Colloquium on Mining in the Vicinity of Geological and Hazardous Structures, which was organized by The South African Institute of Mining and Metallurgy in Randburg on 4th June, 1986.

† Chief of Division, Rock Mechanics Laboratory, Chamber of Mines of South Africa Research Organization, P.O. Box 91230, Auckland Park, 2006 Transvaal.

 ISSN 0038-223X/$3.00 + 0.00.

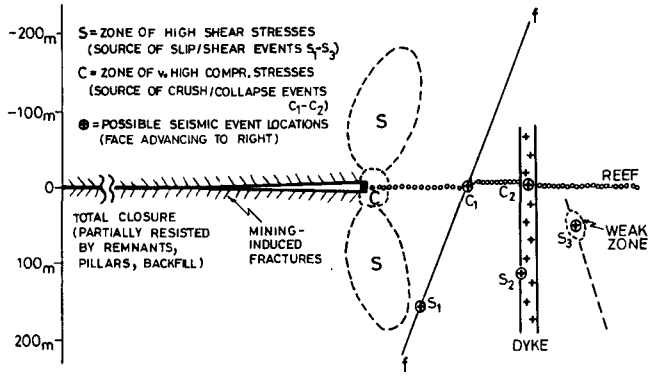

Fig. 1—An isolated stope at depth, showing stresses and foci of seismic events

characterized by very high concentrations of compressive stress. These stresses cause intense fracturing in the rockmass of zone C, traces of which are left behind as the familar face-parallel hangingwall and footwall fractures as the face moves forward. Most of this fracturing takes place quasi-stably: ERR manifesting itself harmlessly in the form of crushing and frictional heating[13,14]. Occasionally, however, a volume of rock may rupture violently as a 'strain burst' in which intense, if localized, damage occurs. The mechanism for such events was likened by Cook[15] in 1965 to behaviour of brittle rock in a 'soft' testing machine: extremely violent failure in such tests is (all too) easy to reproduce in the laboratory. Undoubtedly, the presence or absence of geological features such as dykes or minor faults and joints[5] plays some role in governing the sporadic appearance of these 'crush'-type events—Fig. 1.

Above and below the face in Fig. 1 are also large lobes, S, of moderately high concentrations of shear stress. As the face advances, these lobes sweep through volumes of 'intact' rock, normally leaving no evidence of their passage behind them. Occasionally, however, a lobe will impinge on a pre-existing plane of weakness such as a fault, joint, or dyke contact. Now, the possibility[16] of a class S event arises: sudden and violent slip along the plane. Similarly, if a lobe encounters and activates a suitably orientated zone of weakness somewhere in the rockmass, a damaging planar rupture type of event can be triggered. In general, rockburst damage resulting from shear events is likely to be more widespread, and the event magnitudes larger, than for crush events in that much larger, if more remote, areas of rock are affected—Fig. 1.

It is the latter class S type of event that forms the topic of this paper, but a brief (and in some respects conjectural) summary of the properties of the two notional classes is given in Table I.

Existence of Shear-type Events

Since shear-type rockburst mechanisms are not currently widely invoked by mining rock-mechanics engineers, it is as well to review very briefly the evidence that shear events do, in fact, tangibly occur.

Spottiswoode[17] recently examined the seismograms of 17 events at Blyvooruitzicht Gold Mine, all located in the hangingwall or footwall well removed from the reef plane with magnitudes ranging from 1,0 to 2,1. Few of the events exhibited significant volume changes; instead, all indicated relatively pure shear-type moment tensor contents. This is the norm for earthquakes; apart from seismological calculations, clear traces of earthquake ruptures are often exposed on surface where direct ride dislocations indicate clear-cut shear mechanisms.

In the underground context, numerous natural fault throws indicate that massive ride events took place at some times in the geological past. Rockbursts associated with obvious ride movements on re-activated fault planes were observed recently; one such case is described at the end of this paper. In previously intact rock, burst fractures exhibiting measurable ride movements are also

TABLE I
CHARACTERISTICS OF CLASS C AND CLASS S EVENTS
(Conjectural entries are indicated by [?])

Item	Class C (crush/collapse) events	Class S (slip/shear) events
Physical description	Unstable crushing of volume of rock in close proximity to mining void	Unstable release of shear stress by slip over a planar area (plane of weakness, including 'intact' rock)
Governing mechanism or criterion	Strain-weakening of brittle rock in compression, system stiffness, stress-drop potential, ERR	Static:dynamic shear-stress drop of sliding surfaces, system stiffnesses, stress-drop potential, ESS
Seismic data	Signature: Anomalous dilation signals	Signature: Standard 4-quadrant fault plane solution
	Foci: On or close to face of an excavation [?]	Foci: Off reef plane, typically about 50 to 100 m
	Magnitudes (abutment events): M<2 [?]	Magnitudes: Unbounded, microseisms—M>5+
Common examples	Abutment events, strain bursts, tunnel/dyke events [?]	Most fault and some dyke-related events, earthquakes, most medium to very large events [?]
Rockburst damage	Occasionally intense, but always localized [?]	For larger events: widespread FOG, stope closure/footwall heave, tunnel damage
	Rupture zone trace: Multiple conjugate slip planes or general crushing [?]	Rupture trace: Single quasi-plane showing measurable ride movements

sometimes exposed; one example has been raise-mapped in detail[18]. Such fractures have a 'young' appearance but do not otherwise differ significantly from natural faults: in spite of detailed irregularities including branching, feathering, and *en echelon* features, the overall geometrical effect is a quasi-planar trace permitting the rock-masses on the two sides to ride *en masse* with respect to each other. Again, ride movements and associated shear-type stress relief appear to be the dominant features associated with such events.

Static and Dynamic Friction

As in earthquake theory, the factors governing unstable slip along a plane are, firstly, the prevailing level of shear stresses, which serve to drive the event and, secondly, the friction properties along the plane, which act to inhibit it.

The static friction or 'strength', τ_s, of a relatively smooth pair of contacting rock surfaces tested in the laboratory is shown in Fig. 2. Frictional resistance to slip is commonly found to increase linearly with normal confining stress, σ_N, and is expressed as[19]

$$\tau_s = S_o + \mu_s \sigma_N, \quad \ldots\ldots\ldots\ldots\ldots\ldots\ldots\ldots\ldots\ldots \quad (1)$$

where S_o is a possibly non-zero cohesion, $\mu_s = \tan \phi_s$ is the coefficient of static friction, and ϕ_s is the angle of static friction.

Byerlee[20] published data for a wide range of rock surfaces in which S_o is shown to be nearly zero and μ_s clusters in the range 0,5 to 1,0. This is corroborated by local testing of quartzite[19,21] for which μ_s values near 0,6 ($\phi_s = 30°$) were reported.

The behaviour of actual faults or joints underground may be less clearcut; certainly, mineral infillings or substantial asperities could increase the above values, as shown in Fig. 2. A working hypothesis for *in situ* static strengths might be

$$\tau_s = (0 - 10\,\text{MPa}) + (\tan 30° - \tan 32°)\,\sigma_N. \quad \ldots\ldots \quad (2)$$

Most researchers in earthquake theory agree on the concept of dynamic fraction, τ_d, a reduced level of frictional resistance that pertains once slip has been mobilized and possible macroscopic or microscopic asperities have been sheared off:

$$\tau_d = \mu\sigma_N = (\tan \phi)\sigma_N. \quad \ldots\ldots\ldots\ldots\ldots\ldots\ldots\ldots\ldots\ldots \quad (3)$$

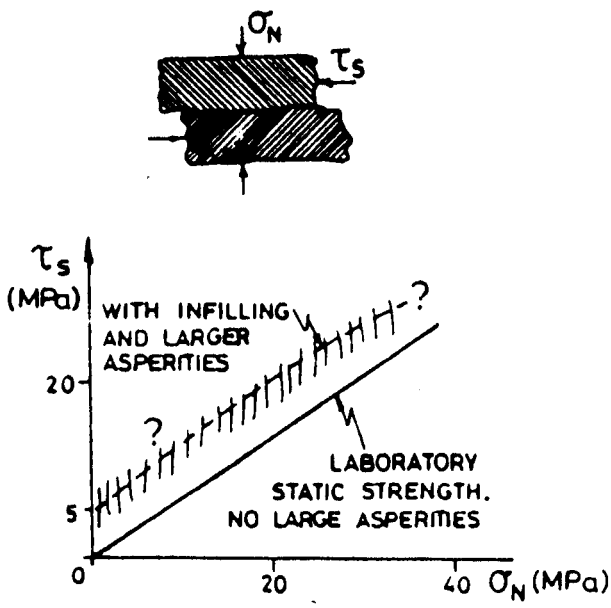

Fig. 2—The static strength of a plane of weakness

Under dynamic conditions, cohesion is said to be negligible and a typical angle of dynamic friction, ϕ, is 30°. The stress drop, τ_e, between equations (2) and (3), illustrated in Fig. 3, has been estimated from mining seismological data[22] to range around 0,1 to 10 MPa, while laboratory stress drops of 5 to 10 per cent have been variously reported[19,23].

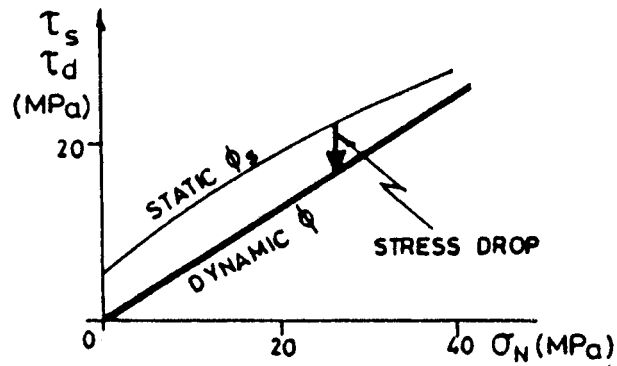

Fig. 3—Static versus dynamic strength and stress drop

A number of diverse explanations for this puzzling drop in friction under dynamic conditions have been advanced[23,24]. There is little doubt, however, that its existence is a necessary factor underlying earthquake ruptures and the mining S-type events discussed here—Fig. 4. Without a finite stress drop, there is no potential for violent shear instability; just as in Cook's[15] model of crush events, violent collapse is impossible if the rock fails in a non-brittle plastic mode without rapid post-failure loss in strength. Clearly, the nature of contacting rock asperities, as well as the presence or absence of gauge, could affect the magnitude and steepness of stress drop along a potentially unstable plane of weakness. This may explain why specifically seismically-active faults are said to be in tight contact and free of gauge[25]. Further careful laboratory testing and back-analysis of actual events from the field are necessary to quantify and explain the stress-drop potential of various planes of weakness. In the meantime, the following are suggested representative values:

$$\hat{\tau}_e \simeq 5 \text{ to } 10\,\text{MPa (unstable plane of weakness)}$$
$$\simeq 20\,\text{MPa (unstable rupture of 'intact' rock).} \quad (4)$$

ESS Genesis of a Slip Event

The following definition sums up the net force available to power a shear type of seismic event once rupture has commenced (Figs. 3 and 4):

Excess shear stress = Prevailing shear stress prior to slip − dynamic strength of plane

$$\text{ESS} = \tau_e = |\tau| - \mu\sigma_N \quad \ldots\ldots\ldots\ldots\ldots\ldots\ldots\ldots \quad (5)$$

Fig. 5 depicts possible shear-stress and friction conditions along a typical rupture plane (joint, fault, or dyke

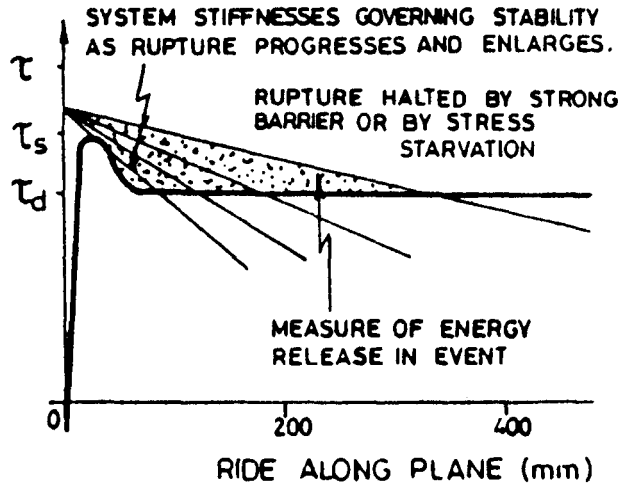

Fig. 4—Stability and stress drop as ride increases beyond a critical amount

contact, Fig. 1). The static resistance to slip or 'strength' of the fault is shown in Fig. 5 as a light irregular line. According to equation (2), this varies, not only with the local normal stress, σ_N, but also, perhaps, extremely erratically owing to changes in μ_s and cohesion along the fault—the effects of major asperities or geometric irregularities of the fault 'plane'.

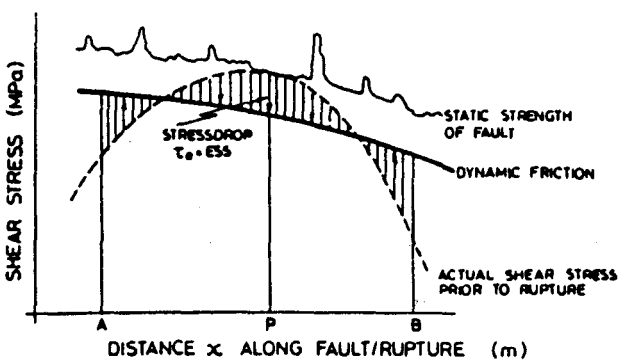

Fig. 5—Strength and stress conditions along a potential rupture plane

However, the heavy line representing dynamic strength (shear resistance once motion over a sensible area of the fault has been mobilized and significant asperities have been sheared off) is depicted in Fig. 5 as a smooth curve, varying only with load σ_N acting along the fault.

The smooth dashed curve in Fig. 5 represents a typical profile of absolute shear stress acting along the fault—virgin stress plus stress induced by the nearby slowly advancing mining excavation. If this stress reaches a value equal to the static strength at some point P along the fault, slip will initiate at that point. By assumption, dynamic friction now pertains and there will be a stress drop, denoted ESS in Fig. 5. This stress drop is unbalanced and therefore forces ride to occur along a small segment of the plane of weakness centred at P. This ride, in turn, generates very large ('infinite') stresses at the tips of the broken segment—stresses sufficient to cause the rupturing segment to grow into regions where the shear stress was previously less than the static strength, even to the extent of rupturing through asperities and other high-strength barriers in the plane. This process is shown in Fig. 6 at a series of time instants during the genesis of the slip event.

In principle, one can fix the final shape of the ride distribution illustrated in Fig. 6 purely from a knowledge of the shaded stress-drop distribution of Fig. 5 by noting that, for static equilibrium, high stresses cannot persist at the tips of the ruptured area. This, in turn, implies that the slope of the ride distribution must be small at these tips, and for numerical calculations it is convenient to set this slope exactly equal to zero[26,27]. Specific examples are given in both mathematical and numerical form later in this paper.

It has been assumed here that the forces and energies needed to *propagate the rupture* are small in relation to the other forces and energies involved. This is certainly true for planes of weakness[28], and is probably true even for significant ruptures of 'intact' rock[28]. A second simplification is that *dilatation effects* of the riding fault have been ignored; under reasonable assumptions, these can be shown to inhibit ride by 10 per cent at the most. A final, more questionable assumption is the neglect of *dynamic effects,* i.e. that the sliding rock surfaces, once set in motion, do not grossly 'overshoot' the bounds AB in Figs. 5 and 6 set by quasi-static equilibrium requirements. Numerical modelling results suggest that overshoot may amount only to about the 20 per cent level[29], and in any event the effects are partially cancelled by the other two simplifications listed above.

With these premises then, the quantity labelled ESS in Fig. 5 and defined in equation (5) is truly the force powering, controlling, and halting dynamic slip events. ESS can readily be calculated by standard stress-modelling programs[10]. It is a convenient single entity that sums up the proclivity for slip on a fault plane, at least in terms of bounding the extent of the area where slip can occur. If the assumptions underlying equations (2) and (3) are accepted, then the peak value of ESS along the plane also serves as a measure of probability of a slip event actually taking place; or, if the peak ESS greatly exceeds, say, 10 MPa, of *already* having taken place.

The complexities of strength variation along the plane (light irregular line in Fig. 5), which would be impossible to quantify in any practical situation, fortunately turn out to be irrelevant once rupture has been initiated. The much smoother and simpler ESS entity is sufficient to define the extent, the potential magnitude and, slightly less precisely, the probability of seismic shear-type activity.

Numerical Evaluation of ESS

A suggested methodology for the numerical calculation and application of ESS in a given mining scenario is as follows.

(i) Decide on the dynamic friction properties of plane. Until better evidence becomes available, a working assumption is $\phi = 30°$.

(ii) Model the appropriate mining geometry with a suitable stress analysis program (e.g. MINAP[30] for 2D situations, MINSIM-D[10] for general single and dislocated reef situations). Components of virgin horizontal stress need to be specified with particular care.

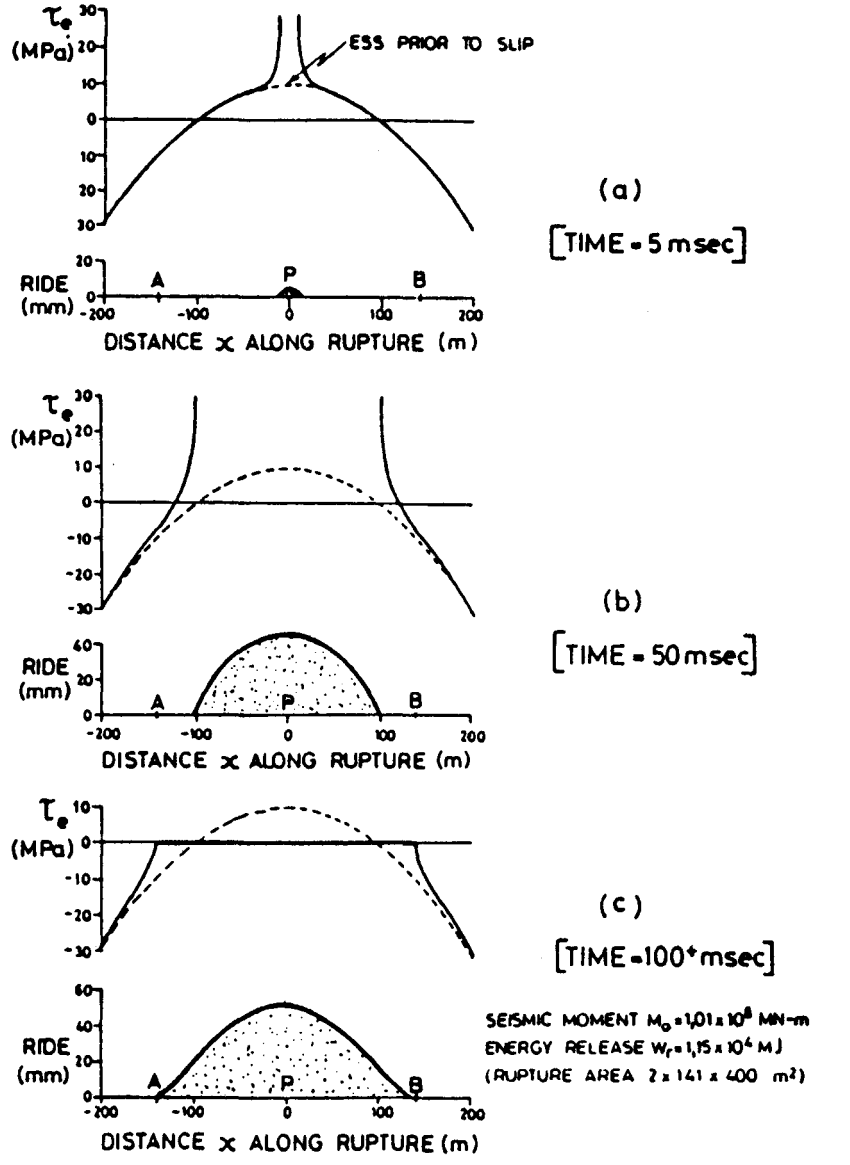

Fig. 6—The genesis of a slip event

(iii) Establish ESS along the chosen plane. (If general stability in an unknown geological environment is to be assessed, a quantity known as Coulomb ESS can be evaluated—Fig. 9a.)

(iv) If positive ESS exists, note the maximum and extent of the positive zone. (Test the maximum for plausibility: if it is greater than 15 MPa for a fault or joint, or perhaps 30 MPa for intact rock, a *prior* event would have occurred and an earlier mining scenario needs to be set up and evaluated. If ESS is less than about 5 MPa, no burst activity is likely; if ESS is less than 0 MPa, no event is possible.)

(v) Estimate the size of the event by means of formulae —Fig. 7, Table II. (Alternatively, directly model the slip by introducing a 'mined' plane with zero stoping width and $\phi = 30°$ along the plane of weakness, and evaluate the seismic moment of resulting ride distribution by use of equation (6).)

(vi) If mining is such that a sequence of events, each temporarily stress-relieving a portion of the fault, can occur over an extended period of time (e.g. stripping along an extensive strike fault or mining through an obliquely striking joint or fault of small throw), these can be simulated by the use of explicit-slip and mining-step features of the modelling programs[10].

(vii) Evaluate the rockburst hazard in terms of the estimated magnitude of the event and distance to nearest workings[31,33].

(viii) Re-plan the mining geometry accordingly, by the use of bracket or stabilizing pillars, backfill, mining re-sequencing.

Examples of ESS studies of this kind appear in companion papers presented at the Colloquium on Mining in the Vicinity of Geological and Hazardous Structures. Much remains to be done in the fronts of laboratory testing and field back-analyses to refine the numerical values and criteria featuring in (i), (ii), (iv), and (vii) above; dependent on the success of this work, improvements to the modelling programs to streamline (v) and (vi) above would be desirable.

In particular, a fundamental defect of ESS analysis that is becoming apparent is its over-conservatism. A typical

mine in which hundreds or even thousands of planes of weakness may exist cannot nor need be exhaustively analysed in ESS terms. What is urgently required are better field or geological indicators of the potential hazard[25] on given structures; mine seismic networks have already indicated their vital contribution towards identifying the subsets of 'hazardous' structures that require special attention on a given mine[3].

Estimation of the Magnitude of an Event

A robust measure[29,32] of magnitude of a shear type of seismic event is the seismic moment, M_o, which is defined by

$$M_o = G\int \text{Ride.d}A = GV = G\bar{R}A \quad \text{(MN-m)}, \quad \ldots (6)$$

where the shear modulus $G = E/2(1+\nu) \simeq 30$ GPa; and the integral can be seen to represent a volume of ride $V = \bar{R}A$, where $\bar{R}$ is the mean ride (m) and A is the area of rupture surface (m^2). The following widely used relationship connects Richter magnitude, M, with M_o:

$$1{,}5M = \log_{10}M_o - 3{,}1. \quad \ldots (7)$$

If rupture energies and dynamic overshoot effects are ignored, the seismic energy release in an event can be estimated from

$$W_k \simeq \tfrac{1}{2}\int \tau_e R dA \quad \text{(MJ)}, \quad \ldots (8)$$

where both stress drop, τ_e, and ride, R, in general vary along the rupturing plane. An average stress drop, $\bar{\tau}_e$, can be defined in terms of equation (8) as

$$\bar{\tau}_e = 2W_k/V = 2GW_k/M_o \quad \text{(MPa)}. \quad \ldots (9)$$

Knowledge of $\bar{\tau}_e$ could be of use in the estimation of maximum particle velocity, v, very close to the source of a slip type of event—information necessary for the design of rockburst-resistant support[31,33]:

$$v = \beta\bar{\tau}_e/G \quad \text{(m/s)}, \quad \ldots (10)$$

where β is seismic shear-wave velocity (typically 3300 m/s).

An empirical, and probably not particularly robust, relationship between Richter magnitude, M, and seismic-energy release has been suggested for use in South African goldfields[22]:

$$1{,}5M \simeq \log_{10}W_k + 1{,}2. \quad \ldots (11)$$

In principle, all the above quantities, particularly the moment and magnitude via equations (6) and (7), can be estimated by numerical modelling of a potential event if explicit slip along the rupture plane is permitted to occur.

A more rapid and convenient procedure permits one to bypass the explicit modelling of slip in a number of fairly common cases. Two conditions must be met: firstly, that the rupture plane does *not* directly intersect a mined-out area and, secondly, that the ESS distribution along the plane roughly approximates either a 2D (rectangular) or a 'circular' outline. The graphs in Fig. 7 then permit rapid assessment of key parameters including M_o, $\bar{\tau}_e$, source dimension (rupture length), L_s, and peak ride, $\hat{R}$. Fig. 7 is based, for the most part, on analytic solutions for slip resulting from certain idealized ESS distributions; mathematical details are given in the Addendum.

Five families of possible ESS distributions are given in Figs. 7(a) to (e). For each family, the leftmost sketch illustrates the appearance of the ESS contour on the plane prior to slip; the solid line indicates the zero ESS contour, the broken line the location of the peak ESS, $\hat{\tau}_e$, and the stylized arrows the orientation of the ESS vector. The next pair of graphs illustrate the ESS profile or section along the x-axis paramatized in various ways, with the resulting ride profile, after slip has occurred, sketched below. The rightmost graph illustrates the variation of key seismic parameters; a particular value of Poisson's ratio $\nu = 0{,}2$ was used to fix the M_o graphs. All the values are in normalized form. To recover absolute quantities, the following multiplying factors need to be applied:

Distances	a (half-width of ESS contour)
Stress drops	$\hat{\tau}_e$ (peak ESS, MPa)
Rides, R	$\hat{\tau}_e a/\lambda$
	($\lambda = E/4(1-\nu^2) \approx 18\,000$ MPa for 2D cases
	$= E(1-\nu/2)/4(1-\nu^2) \approx 16\,000$ MPa for circular cases .... (12)
Moment, M_o	$\hat{\tau}_e a^2 \ell$ for 2D geometries
	$\hat{\tau}_e a^3$ for circular geometries.

The five families cover the following cases:

Fig. 7(a): Symmetrical ESS over a rectangular region, strike length ℓ. The parameter m indicates where ESS reaches half its peak value, thus measuring the squareness or steepness of the driving ESS profile. Curve A represents a prototype simple response of 2D-type slip events.

Fig. 7(b): Skew ESS distribution over a rectangular region. The parameter c indicates the position of the peak ESS $\hat{\tau}_e$ and thus measures the skewness of the ESS profile. Such profiles are common near isolated extensively mined-out areas, the peak ESS being skewed towards the nearest mining face. Ride and magnitudes diminish with increasing skewness. The zero skewness Case 1 degenerates to Case A of the previous family.

Fig. 7(c): Double-peaked symmetric ESS over a rectangular region, parametized by position of the peak $\hat{\tau}_e$. Such profiles are common where extensive mining has taken place on either side of a fault loss. Curve I degenerates to curve B of the first family. Curve III is of particular interest: it illustrates a bounding case of how rupture can break through even a fairly deep 'well' of negative ESS separating two positive areas, although M_o is in fact strongly reduced in this case.

Fig. 7(d): Symmetric ESS over a roughly circular region, parametized by position of the $\hat{\tau}_e/2$ contour. Such simple profiles are perhaps not very common in mining, but they are mathematically tractable and Case C (constant ESS over the rupture area) in fact represents the popular Brune model used in routine seismological estimates[22] of source dimensions. Case A may represent a slightly more realistic ESS distribution for general use in mining seismological calculations. Fig. 8 illustrates represen-

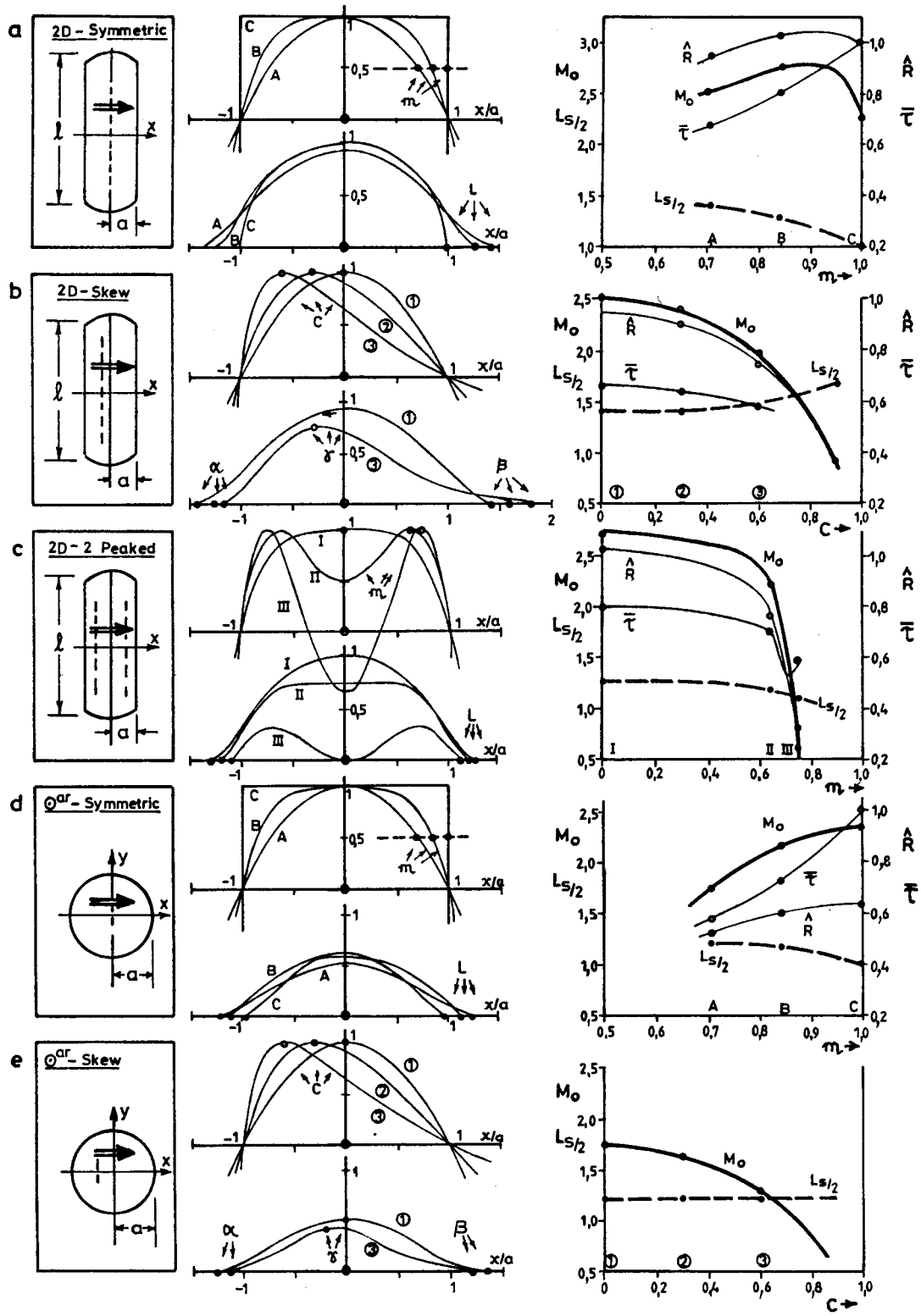

Fig. 7—Ride and seismic parameters for five families of driving ESS profiles

tative relations between M and source dimension/peak ride/average stress drop based on this case; it permits quick assessment of the orders of magnitude likely to be involved in any given event, which can then be supplemented by the more detailed and accurate results of Fig. 7.

Fig. 7(e): Skew ESS over a roughly circular region, parametized by position of peak $\hat{\tau}_e$. This type of profile can arise on obliquely striking planes of weakness transected by mining. Case 1 degenerates to A of the previous family. The calculations for this particular figure were based on partial numerical, rather than purely analytic, modelling—explained in the Addendum.

If one of the above profiles applies then, it is possible by the use of equations (12) and (7) to gain a rapid assess-

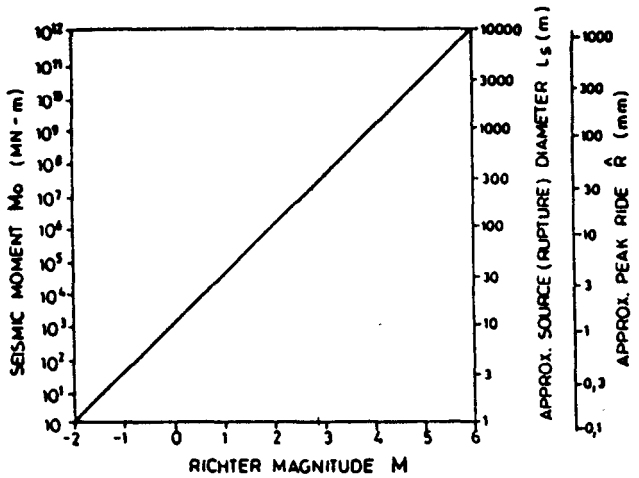

Fig. 8—Seismic moment, M_o, versus Richter magnitude, M (also, indicative source dimension and peak ride for the circular ESS profile of Fig. 7d A with peak stress drop = 10 MPa and mean stress drop = 6 MPa)

ment of the magnitude and rupture area of a potential event. It must be stressed again that the procedure does *not* apply if the rupture breaks through into a mined-out area; in such cases very much greater ride and moment (and stope closure) values will be generated than are indicated in Fig. 7.

ESS Analysis for an Isolated Stope

In this Section, the state of stress and associated shear-event hazard for an isolated stope at depth is briefly reviewed. Salamon's analytic solution[34] for this simple 2D geometry was used to evaluate stresses, and hence ESS distributions, at required points in the solid. This otherwise exact type of analysis suffers from the 'normal' defects of viewing the stope as a mathematical slit of nominal stoping width free of any form of fracturing. These simplifications are not thought to affect the calculated stress distributions significantly at distances greater than about 20 m from the stope excavation.

Fig. 9(a) illustrates the state of footwall shear stress expressed[19] in terms of Coulomb ESS vectors, the size of vector being proportional to the *maximum* magnitude of ESS at a point, and the orientations indicating the conjugate directions along which the probability of slip is maximized. In a compressive-stress field, in terms of principal stresses σ_1 and σ_3,

$$\text{Coulomb maximum ESS} = \sec\phi\cdot(\sigma_1-\sigma_3)/2 - \tan\phi(\sigma_1+\sigma_3)/2$$
$$= 0{,}866\ \sigma_1(0{,}333 - \sigma_3/\sigma_1) \quad \text{for } \phi = 30^\circ \ \ldots\ldots (13)$$

$$\text{Orientation to } \sigma_1 = \pm(45^\circ - \phi/2)$$
$$= \pm 30^\circ \text{ for } \phi = 30^\circ.$$

This form of plot is useful in two ways. Firstly, the size of the lobe in which the ESS is active is clearly depicted; outside this lobe no shear-type events are in theory possible. Secondly, the preferred orientations of slip planes are highlighted; for example, behind the face, bedding-plane slip appears possible while, if the face is advancing towards the right, the first planes of weakness that would most strongly be activated would dip at approximately 70°. Similar conditions, in a mirror-image sense, exist in the hangingwall region above the face.

Fig. 9(b) shows ESS contours for planes dipping at specifically 70°. Three tangents to these contours are illustrated; they indicate the most probable relative point of initiation of slip events for the face advancing to the right for three possible maximum stress drops: $\hat{\tau}_e = 10$, 5, and 2 MPa. Also indicated are the associated lengths of rupture and event magnitudes based on the results of Fig. 7(b), whose 'skew' driving ESS profiles closely match the actual profiles of Fig. 9(b). A strike distance of activated fault $\ell = 2L_s$ (twice the rupture length) was assumed throughout.

Figs. 10(a) and 10(b) illustrate the results of a sensitivity study, varying a number of parameters in relation to a 'base' case having depth $H = 4000$ m, stope half-span L = 200 m, stoping width = 1 m, horizontal-to-vertical stress ratio $k = 0{,}5$, and angle of dynamic friction $\phi = 30^\circ$. In all cases, maximum slip activity occurs for rupture-plane dip angles close to 70° or 130°. This orientation, as well as the disposition of the associated rupture planes —Fig. 9(b)—which initiate far removed from the reef elevation and do not break into the stope or across the reef plane, are loosely substantiated by field data of a number of typical rockburst ruptures[17,18,35] in the important magnitude range $M = 1$ to 2.

The effect of changes in various parameters indicates some interesting, even paradoxical, trends. The reduction of the effective stoping width to 0,5 m (for example by the use of backfill or stabilizing pillars) strongly

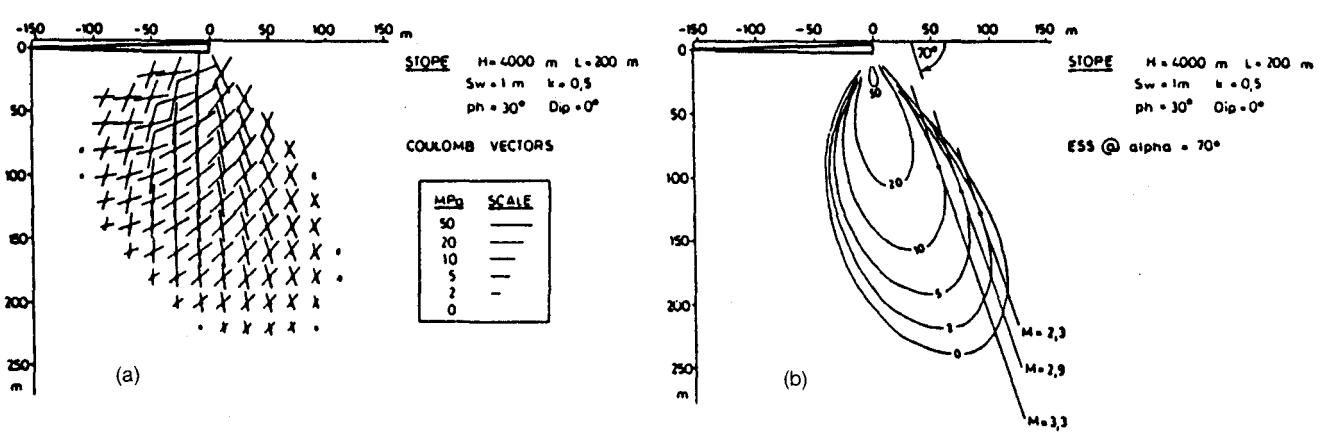

Fig. 9—Isolated stope. Footwall Coulomb and 70° ESS lobes

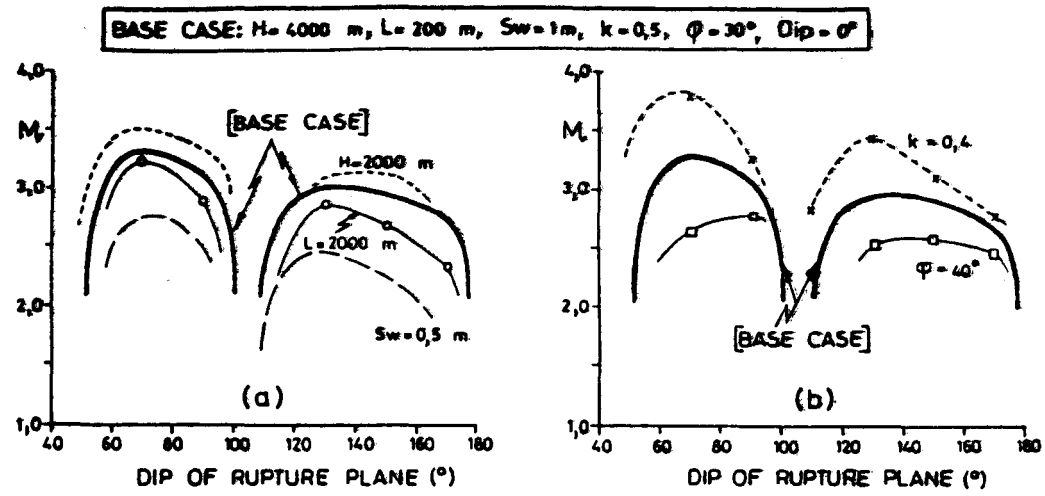

Fig. 10—Isolated stope. Sensitivity of event magnitudes to variation of geometric and other parameters

reduces the event magnitudes as expected, since the stope closures and ERR are reduced in proportion. Equally predictably, changes to the friction angle or the *k*-ratio strongly affect the proclivity for slip. Natural variations in these parameters doubtless help explain why certain geological structures are more burst-prone than others. The sensitivity to *k*-ratio is particularly significant, and this topic is discussed further in the next Section. The effect of dip of the mined strata is to reduce potential magnitudes in the footwall but enhance them in the hangingwall in respect of the down-dip abutment; the same effect is seen in isolated dipping remnants (not illustrated here).

More paradoxically, however, a massive increase in the mined half-span to 2000 m leads to a slight *reduction* in event magnitudes; this is because, while the intensities of the shear stresses are increased, the size of the ESS lobe is actually reduced because of the smaller open zone in the stope. A reduction in depth from 4000 to 2000 m leads to an even more startling result: the magnitudes of the events *increase*. Conversely, an increase in the depth of mining of an isolated stope should in theory be accompanied by a *reduction* in the magnitude of the associated events—an observation, which, if true, holds out some encouragement for the long-term trend of the industry towards the extraction of ultra-deep orebodies.

These more paradoxical findings, which are at variance with standard simple ERR predictions, are a direct consequence of the fact that, for a given stress drop, $\hat{\tau}_e$, the seismic moments are proportional to the *square* (or for circular profiles, the *cube*) of the size of the ESS lobe—equation (12). Lobe size, which measures the extent of the zone disturbed by mining-induced stresses, therefore dominates the control of the size of associated events, although it is presumably true that the *frequency/probability* of events occurring is influenced by the intensity of the ESS occurring in the centre of a given lobe. Thus, for example, large-span deep excavations could be expected in general to be accompanied by more frequent events, but of lower maximum magnitude. This observation is not well-substantiated by seismic or other data; part of the reason for this may be the over-riding effect of virgin *k*-ratio variations, which are discussed below.

Virgin Horizontal Stresses

In traditional ERR-orientated stress modelling, virgin horizontal stresses (*k*-ratios) have relatively little numerical impact. Accordingly, the importance of having reasonably realistic estimates of these stresses has tended to be discounted. However, Fig. 10 and equation (13) suggest that virgin horizontal stresses can have a strong bearing on shear stresses in general, and on mining-induced ESS magnitudes and lobe sizes in particular.

Even in the absence of mining, it is easy to show that a 'critical *k*-ratio' must exist. Consider a mass of elastic ground transected by planes or zones of weakness having friction angle ϕ. Standard Coulomb analysis—equation (13)—shows that these planes will be *unstable* if they are cohesionless and the horizontal stress falls below the value

$$\sigma_3 = \frac{1 - \sin \phi}{1 + \sin \phi} \sigma_1, \quad \text{..... (14)}$$

i.e. $k_{crit} = 0{,}33$ for $\phi = 30°$.

In other words, if for any reason the virgin-stress ratio falls below k_{crit}, massive slip events (normal faulting) must takes place over geological time to relax regional shear stresses, and thereby increase virgin horizontal stresses and *k*-ratios to more stable values. (This is a fairly standard geotectonic or seismological view of faulting, although researchers sometimes work with maximum shear stress, $(\sigma_1 - \sigma_3)/2$, rather than with the more appropriate Coulomb stresses of equations (13) and (14).)

Alternatively, if virgin *k* values are close to k_{crit}, then the ground is stable only by virtue of its non-zero cohesion. Mining in such areas will generate very large ESS lobes, and these could in principle trigger very large events. This, then, identifies another form of 'hazardous structure' not currently widely recognized. The presence of a low virgin *k*-ratio is hazardous in its own right, without *necessarily* being associated with obvious geological structures or planes of weakness.

Fig. 11 illustrates some measurements of virgin stress in South African goldfields, as reported by Gay and McGarr[36]. Horizontal virgin stresses show considerable scatter, due as much perhaps to experimental difficulties as to genuine differences in local tectonic conditions. However, the solid dots should be noted: these show consistent behaviour of σ_3 in a particular district and actually indicate a potential hazard of the above type. Pockets of low (or very high, *k* greater than 3) horizontal stresses may also exist in geologically highly disturbed areas in

the Klerksdorp and Orange Free State goldfields. In these cases, a better knowledge of horizontal stresses, gained through an ordered campaign of *in situ* measurements of virgin stress, seems to be warranted. With such knowledge, appropriate remedial designs could in principle be adopted: the orientation of faces oblique to minor principal stress direction, the use of bracket or stabilizing pillars or backfill, and so on.

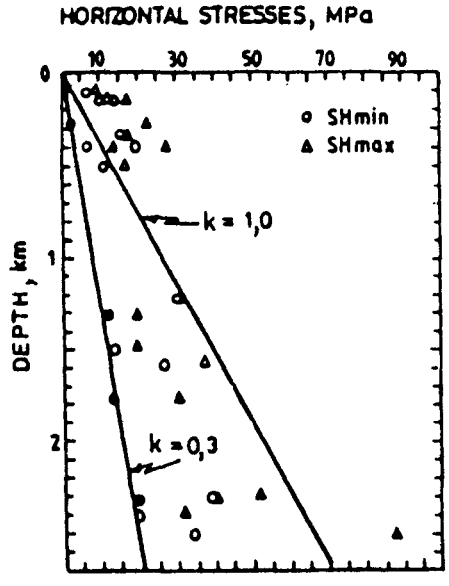

Fig. 11—Virgin horizontal stresses in South African goldfields (after McGarr and Gay[36])

A further aspect of Fig. 11 is worth mentioning. Horizontal stresses at shallow depth tend to be relatively large—a worldwide trend[36]. This doubtless helps to explain why very large mining-related events, predicted by Fig. 10(a) for a fixed k-ratio of 0,5, occur only very rarely at moderate depth, where actual k-ratios greater than 1,0 usually pertain. Conversely, if Fig. 11 can be construed to bound the likely k-ratios at great depth to about 0,5 or greater, then the conclusions of the previous section as to the non-increase of relative hazard associated with ultra-deep mining may be substantiated.

Back-analysis of Selected Events

Two particularly large events are reviewed here; other examples of back-analyses are reported in accompanying papers in the Colloquium on Mining in the Vicinity of Geological and Hazardous Structures.

The first event (January 1983, magnitude 4,0) took place in a graben structure at a gold mine in the Klerksdorp district, Fig. 12. The event was unusual, not only in terms of its magnitude, but in that an unequivocal trace of the burst rupture was exposed in a new haulage driven to re-open the heavily damaged workings of the down-faulted lower reef plane. The burst trace illustrated[37] in Fig. 12 was located in previously intact ground a few metres north of the original crosscut. The average dip was estimated at 60°, and enormous ride dislocations totalling 600 mm were evident over the shear-zone width of about 8 m. Back-analysis of this event proved difficult, not least because of the complex geology of the area. The ESS distribution over the projected rupture plane indicated a fair potential for slip, and a reasonably clear-cut role of mining of the lower reef as the triggering mechanism for the event. However, only by a reduction of the local k-ratios to 0,3, or by permitting the rupture to propagate into the upper extensively worked-out and now-inaccessible areas, was it possible to account for the large Richter magnitude and ride values of this event.

The second event (April 1982, magnitude 4,5) took place on the Wesselia fault complex in the Orange Free State goldfields. The effects of the burst, which included damage to two shafts, were widespread, though fortunately not exceptionally intense. Clear traces of the associated ride movements are still visible in the form of gradeline, track, and drain dislocations in numerous haulages transecting the fault; these have recently been mapped[38] and appear here in the form of Fig. 13. ESS back-analysis[39] clearly substantiates the area of observed movement, including indirect verification of some areas where movement did *not* occur—Fig. 13. Explicit-slip modelling, Fig. 13, also gives reasonable substantiation of the observed magnitudes of ride, which would perhaps fit even more precisely if the assumed angle of dynamic friction were dropped slightly. In this example, it was again necessary to assume that slippage moved into and

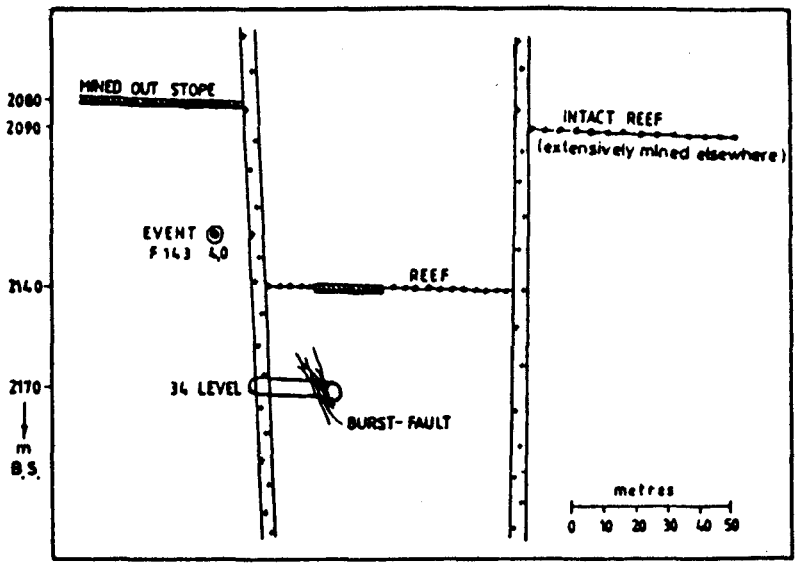

Fig. 12—Location of a graben-burst rupture

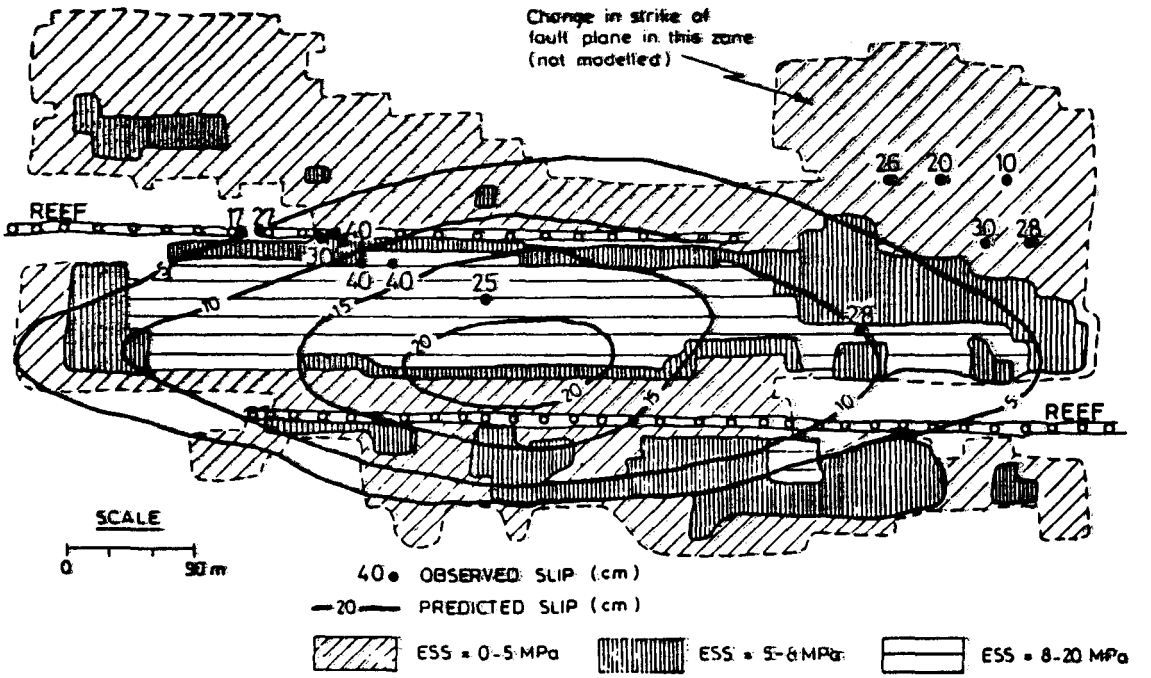

Fig. 13—Wessella event—observed and modelled slip and ESS magnitudes

caused additional closure of the mined-out areas. This is reasonable here since mining in the upper and lower horizons had completed stripping-out along virtually the entire fault plane.

These two examples are atypical in the magnitudes of the events involved, and neither in fact permitted the simplified formulae of Fig. 7 to be applied. They did, however, serve to shed some light on the relevance of shear-stress control of certain types of large seismic events or rockbursts. As already discussed, further back-analyses of more diverse events could help to refine and quantify the key parameters needed for application to pragmatic design problems.

Conclusions

(1) Seismic events and associated rockbursts may fall into at least two distinct categories. Shear-controlled events form an important class.

(2) Excess shear stress, ESS, is a useful measure of driving shear stress, which in principle controls the initiation, propagation, and termination of shear-type events. ESS analyses could usefully be used to supplement (*not* supplant) ERR studies, particularly in geologically disturbed areas.

(3) The key parameters needed in ESS studies are the angle of dynamic friction and the likely maximum stress drop, for which representative values for planes of weakness may be 30° and 10 MPa. Further laboratory testing, field back-analyses, and geological or seismological correlation studies are needed to confirm these values for application to practical situations.

(4) Numerical modelling can readily be harnessed to carry out ESS analyses. Explicit-slip modelling with ϕ preset to its dynamic value permits the assessment of the possible magnitudes of events in complex mining layouts. Alternatively, simplified formulae permit the rapid estimation of event parameters in a number of practical situations.

(5) Low (or extremely high) states of virgin horizontal stress in any given locale constitute a mining hazard in their own right. Conversely, if virgin horizontal stresses increase steadily with depth so that k is greater than 0,5, large-event hazards of ultra-deep mining are possibly bounded. Further *in situ* stress measurements correlated with associated seismicity are needed to shed light on these potentially important aspects.

(6) A guiding principle in the application of ESS to mine design seems to be to aim to limit the *extent* of mining-induced disturbance zones as measured by the size of corresponding positive ESS lobes. Methods for accomplishing this include already well-established procedures such as the use of bracket pillars, stabilizing pillars, or backfill, the correct orientation of faces, and the correct sequencing in the extraction of neighbouring panels. ESS provides a potentially useful measure for the *quantification* of these procedures, and the tangible accomplishment of this aim forms a challenge for the future.

Acknowledgement

The work embodied in this paper formed part of the research programme of the Chamber of Mines of South Africa Research Organization.

Addendum: Functions Underlying Fig. 7

The normalizations used throughout are given in equation (12), and the notation is indicated in the text accompanying Fig. 7. In the following, radius L denotes the half-span of rupture in the direction of ride for both 2D and circular ESS geometries. The integrals involved are simplest if the coordinate system has its origin at the centre of the *rupture* profile. Finally, the results have been converted to a system with the origin at the centre of the driving τ_e profile and re-normalized to give a unit-peaked τ_e with unit radius as in Fig. 7. In the following, single integrals indicate 2D geometries, double integrals circular geometry (where ρ and ϕ are polar coordinate

forms of x and y).

By the Reciprocal Theorem[19], the volume of ride, V, and hence the seismic moment, M_o, are given by

$$V = \int_{-L}^{L} \sqrt{(L^2-x^2)}\tau_e(x)dx$$

$$= \frac{2}{\pi} \int_{-\pi}^{\pi} \int_{o}^{L} \sqrt{(L^2-\rho^2)}\tau_e(\rho,\phi)\rho d\rho d\phi. \quad \text{..... (A1)}$$

Ride, when τ_e is a polynomial (cases a, c, d), takes the form of a polynomial-multiplier of the constant-excitation solution[40], and general forms can be evaluated by the use of standard on-reef kernels in 2D and 3D. (Salamon's simplification[40] of ride kernels was applied in case e.)

$$\tau_e(x) = \frac{1}{\pi} \int \frac{[\zeta^n\sqrt{(L^2-\zeta^2)}]}{(\zeta-x)^2} d\zeta$$

$$\tau_e(x,y) = \frac{1}{2\pi} \iint \frac{\left[\frac{2}{\pi}\rho^n\sqrt{(L^2-\rho^2)}\right]}{[(\zeta-x)^2+(\eta-y)^2]^{3/2}} d\zeta d\eta. \quad \text{.... (A2)}$$

For static equilibrium, ride has zero slope at L (equivalently, induced stress is non-infinite at the rupture tips); this implies a zero factor in the numerator polynomial of the R distributions and permits L to be evaluated accordingly. The mean stress drop is found from equations (8) and (9). A summary of the results is given in Table II.

References

1. *Fifth report on statistical analysis of practical data on rockbursts—An analysis of the influence of dykes, faults and raises on the incidence of rockbursts.* South African Council for Scientific and Industrial Research, N281, Oct. 1959. 59 pp.
2. COOK, N.G.W., HOEK, E., PRETORIUS, J.P.G., ORTLEPP, W.D., and SALAMON, M.D.G. Rock mechanics applied to the study of rockbursts. *J.S. Afr. Inst. Min. Metall.*, May 1966. pp. 506–516.
3. GAY, N.C., SPENCER, D., VAN WYK, J.J., and VAN DER HEEVER, P.K. The control of geological and mining parameters on seismicity in the Klerksdorp gold mining district. *Proceedings Symposium on Rockbursts and Seismicity in Mines.* Johannesburg, The South African Institute of Mining and Metallurgy, 19°4. pp. 107–120.
4. JOUGHIN, N.C. The measurement and analysis of earth motion resulting from underground rock failure. Ph.D. thesis, University of the Witwatersrand, 1966.
5. RORKE, A.J., and ROERING, C. Source mechanism studies of mining-induced seismic events in a deep level gold mine. *Proceedings Symposium on Rockbursts and Seismicity in Mines.* Johannesburg, The South African Institute of Mining and Metallurgy, 1984. pp. 51–56.

TABLE II

ANALYTIC FUNCTIONS FOR SEISMIC PARAMETERS IN TERMS OF τ_e PROFILE

ESS profile τ_e	Ride R	Rupture length L_s	Seismic moment $M_o/\pi(l-\nu)$
a *2D-Symmetric* $(1-x^{2n})$ $n=1,2,\ldots\infty$ $m^{2n} = ½$	$\frac{x^{2n-2}}{2n+1}\sum_{r=0}^{n-1}\left(\frac{-3/2}{r}\right)\left(-\frac{L^2}{x^2}\right)^r [L^2-x^2]^{3/2}$ $R_1(x) = ⅓[2-x^2]^{3/2}$; $R_\infty(x) = [1-x^2]^{½}$	$L_s = 2L$ $L^{2n} = (1)_n/(½)_n$	$\frac{2n}{2n+2}L^2$
b *2D-Skew* $(1-c^2)\frac{1-x^2}{(1+cx)^2}$	$\frac{\delta R}{\delta x} = -(1-c^2)\frac{(\gamma+x)\sqrt{(\beta-x)(\alpha+x)}}{(1+cx)^2}$ $\gamma = (1-\sqrt{1-c^2})/c$	$L_s = \alpha+\beta$ $\binom{\alpha}{\beta} = \sqrt{2\gamma^2+2} \mp \gamma$	$(1-\gamma^2)^2$
c *2D-2 Peaked* $\frac{4}{1+t^2}(1-x^2)(t+x^2)$ $-0{,}115<t<1$ $m = \sqrt{(1-t)/2}$	$\frac{0{,}8}{(1+t)^2}\left[x^2+\frac{3}{2}L^2-\frac{5}{3}(1-t)\right]\left[L^2-x^2\right]^{3/2}$	$L_s = 2L$ $g^2 = (1-t)^2+6t$ $L^2 = ⅔(1-t+g)$	$L^4\frac{L^2-1+t}{(1+t)^2}$
d *Circular-Symmetric* $(1-\rho^{2n})$ $n=1,2,\ldots\infty$ $m^{2n} = ½$	$\frac{2}{\pi}\left[\frac{(1)_n}{(3/2)_n}\right]^2\rho^{2n-2}\sum_{o}^{n-1}\left(\frac{-3/2}{r}\right)\left(-\frac{L^2}{\rho^2}\right)^r [L^2-\rho^2]^{3/2}$ $R_1(\rho) = \frac{8}{9\pi}\left[\frac{3}{2}-\rho^2\right]^{3/2}$; $R_\infty(\rho) = \frac{2}{\pi}[1-\rho^2]^{½}$	$L_s = 2L$ $L^{2n} = (3/2)_n/(1)_n$	$\frac{2}{3(1-\nu/2)}\frac{2n}{2n+3}L^3$
e *Circular-Skew* $(1-c^2)\frac{1-x^2-(y/\hat{y})^2}{(1+cx)^2}$	Not evaluated	$L_s = \alpha+\beta$ $\alpha, \beta, \hat{y}$ chosen to minimize rim stresses $0{,}95<\hat{y}<1{,}0$ in Fig. 7e	Use of equation (A1)

6. VAN DER HEEVER, P.K. Some technical and research aspects of the Klerksdorp seismic network. *Ibid.*, pp. 349–350.
7. ADAMS, G.R., JAGER, A.J., and ROERING, C. Investigations of rock fracture around deep-level gold mine stopes. *Proceedings 22nd U.S. Symposium on Rock Mechanics, Rock Mechanics from Research to Application.* Boston, Massachusetts Institute of Technology, Jun./Jul. 1981.
8. SALAMON, M.D.G., and WAGNER, H. Role of stabilizing pillars in the alleviation of rockburst hazard in deep mines. *Proceedings Fourth International Congress, International Society of Rock Mechanics.* Montreaux, 1979. vol. 2, p. 564.
9. PIPER, P.S. An assessment of backfilling to provide regional support in deep mines. Unpublished material, Jul. 1985.
10. RYDER, J.A., and NAPIER, J.A.L. Error analysis and design of a large-scale tabular mining stress analyser. *Proceedings Fifth International Conference on Numerical Methods in Geomechanics.* Nagoya, Apr. 1985. pp. 1549–1555.
11. JOUGHIN, N.C., and JAGER, A.J. Fracture of rock at stope faces in South African gold mines. *Proceedings Symposium on Rockbursts—Prediction and Control.* London, Institution of Mining and Metallurgy, 1983.
12. STILLER, H., HURTIG, E., GROSSER, H., and KNOLL, P. On the nature of mining tremors. *J. Earthq. Predict. Res., Tokyo,* vol. 2, 1983. p. 61.
13. BRUMMER, R.K. Fracturing and deformation at the edges of tabular gold mining excavations and the development of a numerical model describing such phenomena. Ph.D. thesis, Rand Afrikaans University, 1986. (In preparation.)
14. LEGGE, N.B. Rock deformation in the vicinity of deep gold mine longwall stopes and its relation to fracture. Ph.D. thesis, University of Wales (Cardiff), 1984.
15. COOK, N.G.W. A note on rockbursts considered as a problem of stability. *J.S. Afr. Inst. Min. Metall.,* Mar. 1965. pp. 515–523.
16. RYDER, J.A., LING, T., and WAGNER, H. Slippage along a fault plane as a rockburst mechanism—static analysis. Unpublished material, Jun. 1978.
17. SPOTTISWOODE, S.M. Source mechanisms of mine tremors at Blyvooruitzicht Gold Mine. *Proceedings Symposium on Rockbursts and Seismicity in Mines.* Johannesburg, The South African Institute of Mining and Metallurgy, 1984. pp. 29–38.
18. ORTLEPP, W.D. The mechanism of a rockburst. *Proceedings 19th U.S. Symposium on Rock Mechanics.* Kim, Y.S. (ed.). Reno, University of Nevada, 1978. p. 476.
19. JAEGER, J.C., and COOK, N.G.W. *Fundamentals of rock mechanics.* London, Chapman & Hall, 1969. pp. 56, 59, 62, 65, 87–91.
20. BYERLEE, J. Friction of rocks. *Proceedings Second Conference on Experimental Studies of Rock Friction with Application to Earthquake Prediction.* Menlo Park, U.S. Dept. of the Interior, Office of Earthquake Studies, 1977. pp. 55–79.
21. BRUMMER, R.K., and TAGGART, P.N. Personal communication, Mar. 1986.
22. SPOTTISWOODE, S.M., and McGARR, A. Source parameters of tremors in a deep-level gold mine. *Bull. Seism. Soc. Am.,* vol. 65. 1975. pp. 93–112.
23. DIETERICH, J.H. Time-dependent friction and the mechanics of stick-slip. *Proceedings Second Conference on Experimental Studies of Rock Friction with Application to Earthquake Prediction.* Menlo Park, U.S. Dept. of the Interior, Office of Earthquake Studies, 1977. pp. 81–115.
24. SCHOLTZ, C.H., and ENGELDER, J.J. The role of asperity indentation and ploughing in rock friction. I Asperity creep and stick-slip. *Int. J. Rock Mech. Min. Sci.,* vol. 13, no. 5. 1976. pp. 149–154.
25. VAN DER HEEVER, P.K. Personal communication, Apr. 1986.
26. NUR, A. Nonuniform friction as a physical basis for earthquake mechanics: a review. *Proceedings Second Conference on Experimental Studies of Rock Friction with Application to Earthquake Prediction.* Menlo Park, U.S. Dept. of the Interior, Office of Earthquake Studies, 1977. pp. 262–264.
27. RYDER, J.A. Rational function analysis of tabular excavations in two dimensions (Green functions, energy release rate, error analyses and edge corrections, soft-seam kernels). Unpublished material, Jul. 1984.
28. DMOWSKA, R., and RICE, J.R. Fracture theory and its seismological applications. *Continuum theories in solid earth physics.* Teisseyre, R. (ed.). Poland, Elsevier, 1983.
29. AKI, K., and RICHARDS, P.G. *Quantitative seismology.* San Francisco, W.H. Freeman, 1979. p. 880.
30. CROUCH, S.L. Analysis of stresses and displacements around underground excavations: an application of the displacement discontinuity method. University of Minnesota, *Geomech. Report,* Nov. 1976.
31. McGARR, A. Some applications of seismic source mechanism studies to assessing underground hazard. *Proceedings Symposium on Rockbursts and Seismicity in Mines.* Johannesburg, The South African Institute of Mining and Metallurgy, 1984. pp. 199–208.
32. HANKS, T.C., and KANAMORI, H. A moment magnitude scale. *J. Geophys. Res.,* vol. 84. 1979. pp. 2348–2350.
33. WAGNER, H. Support requirements for rockburst conditions. *Proceedings Symposium on Rockbursts and Seismicity in Mines.* Johannesburg, South African Institute of Mining and Metallurgy, 1984. pp. 209–218.
34. SALAMON, M.D.G. Two dimensional treatment of problems arising from mining tabular deposits in isotropic or transversely isotropic ground. *Int. J. Rock Mech. Min. Sci.,* vol. 5. 1968. pp. 159–185.
35. ORTLEPP, W.D. Personal communication, 1985.
36. McGARR, A., and GAY, N.C. State of stress in the Earth's crust. *Ann. Rev. Earth Planet. Sci.,* vol. 6. 1978. pp. 405–436.
37. VAN DER HEEVER, P.K. Personal communication, 1983.
38. MENDECKI, A. Personal communication, Jan. 1986.
39. O'HARE, M. Unpublished material, Feb. 1986.
40. SALAMON, M.D.G. Elastic analysis of displacements and stresses induced by mining of seam or reef deposits, Part IV: Inclined Reef. *J.S. Afr. Inst. Min. Metall.,* Dec. 1964. pp. 319–338.

TABLE II (continued)

Mean stress drop $\overline{\tau}_e$	Peak ride $\hat{R}$
$\frac{2n}{2n+1}$	$\frac{2n}{2n+1} L$
Not evaluated	$\frac{4(1-c^2)}{c^3} [\sin^{-1}\sqrt{\gamma c} - \sqrt{c(c-\gamma)}]$
$\frac{2}{15(1+t)^2} \left[18t + \frac{L^2g^2}{L^2-1+t}\right]$	$\frac{8}{15} \frac{g^{5/2}}{(1+t)^2}$ $t<0,27$ $\frac{4L}{15} \frac{(1-t)L^2+12t}{(1+t)^2}$ $t>0,27$
$\frac{4n}{4n+3}$	$\frac{2}{\pi} \frac{2n}{2n+1} L$
Not evaluated	Not evaluated

binder, and pelletization of the resulting material. The briquettes are analysed with a fully automated X-ray-fluorescence spectrometer, corrections being made for spectral-line overlap and background factors.

The lower limit of detection was 1,5, 2,1, and 2,0 μg/g for U_3O_8, molybdenum, and arsenic respectively. The relative standard deviation did not exceed 0,016 for U_3O_8 up to 1250 μg/g, 0,068 for molybdenum up to 12,4 per cent, and 0,045 for arsenic up to 1,21 per cent. The accuracy of the method compares favourably with that of other methods.

● **Report M322**

The interfacing of a microcomputer with a simultaneous atomic-emission spectrometer, by G.L. Moore, R.L. Paul, and D.R. Groot. Aug. 1987. 12 pp.

Two Hilger Analytical E1000 simultaneous atomic-emission spectrometers have been successfully interfaced to Apple IIe microcomputers. Each microcomputer starts the spectrometer, controls the potentials applied to the photomultiplier tubes, and processes the intensity data. The software, which was written in assembler language and BASIC, allows for 36 analytical methods, each containing up to 30 analytes and using from 3 to 6 calibration standards. Internal standardization is an option on all channels. Intensity data for 396 integrations for all channels are stored on magnetic disc, and can be recalled for use in the analytical program. Calibration graphs can be viewed on the monitor display or printed out.

● **Report M323**

The development and evaluation of a prototype instrument for the measurement of carbon concentration in pulp, by A.E. Holton. Sep. 1987. 22 pp.

Carbon-in-pulp (CIP) is an important process for the recovery of gold on modern plants. This report describes the development and testing of a prototype system that measures the concentration of carbon in CIP adsorption tanks. This measurement can then be used in the control of the carbon inventory.

The instrument consists of a submersible probe coupled to an external electronic circuit and an on-board computer facility. The probe comprises two sections: ultrasound-attenuation transducers, and a density-probe transducer, which measures pulp density by a technique of impedance mismatch. The prototype instrument measures the attenuation of ultrasound in CIP, and this result is used, together with measurements of pulp density and temperature, in an algorithm for the computation of the concentration of carbon.

● **Report M324**

The use of lithium tetraborate in the fire-assay procedure with nickel sulphide as the collector, by R.V.D. Robért. Jul. 1987. 15 pp.

The platinum-group metals were determined in chromite materials by a fire-assay procedure in which lithium tetraborate was substituted for sodium tetraborate in the flux mixture.

The results show that, while lithium tetraborate improves the dissolution of the chromite grains and is more efficient as a fluxing agent than sodium tetraborate, the values obtained for the platinum-group metals are not significantly different. Nevertheless, lithium tetraborate was found to be the preferred reagent for chromium-rich materials. Stages of the analytical procedure at which loss of the platinum-group metals may occur are identified, and recommendations are made as to how these losses can be reduced.

A revised analytical laboratory method is detailed in an appendix.

● **Report M327**

An assessment of the IL 440 atomic-vapour accessory for the determination of gaseous hydride-forming elements by atomic-absorption spectrometry, by G.D. Marshall and U. Grimbeek. Sep. 1987. 13 pp.

The optimum experimental conditions for the determination of antimony, arsenic, bismuth, selenium, tellurium, and tin were established by the simplex method. The experimental parameters that were optimized were acid concentration, amount of sodium borohydride, reaction time, and flowrate of the purge gas.

The optimum conditions were then used in a determination of the working range, detection limit, reproducibility, and measurement time for each analyte. The IL 440 atomic-vapour accessory proved to be a versatile apparatus, which is simple to operate and which yields precise and sensitive results.

A laboratory method is detailed in an appendix.

● **Special Publication no. 9**

Handbook on the estimation of metallurgical process costs, by W.T. Ruhmer. May 1987. 93 pp. R65 incl. postage, US$65 to overseas destinations.

This handbook provides simple techniques for the preliminary estimation of capital and operating costs in extractive metallurgical processes that are of an ore-dressing or hydrometallurgical nature. The following areas are covered: transportation, storage, washing and screening, crushing, grinding, gravity concentration, thickening, leaching, liquid–solid separation, residue disposal, clarification, precipitation, recovery, carbon-in-pulp, flotation, pyrite roasting, calcining, and smelting.

Although the handbook deals mainly with gold-recovery plant and processes, it is also applicable to a wide range of metallurgical and mineral-processing operations. It should prove useful to engineers and students involved in project evaluation because it enables an investigator, with the minimum of effort, to take the first step in deciding whether a project warrants further attention or not.